Earth and Planetary Science Letters 289 (2010) 134–144

Contents lists available at ScienceDirect

Earth and Planetary Science Letters

journal homepage: www.elsevier.com/locate/epsl

Landscape form and millennial erosion rates in the San Gabriel Mountains, CA

Roman A. DiBiase [a,*], Kelin X. Whipple [a], Arjun M. Heimsath [a], William B. Ouimet [b]

[a] School of Earth and Space Exploration, Arizona State University, Tempe, AZ 85287, USA
[b] Department of Geology, Amherst College, Amherst, MA 01002, USA

ARTICLE INFO

Article history:
Received 28 May 2009
Received in revised form 16 October 2009
Accepted 26 October 2009
Available online 22 November 2009

Editor: Dr. R.W. Carlson

Keywords:
erosion
landscape evolution
topographic metrics
cosmogenic radionuclides
San Gabriel Mountains

ABSTRACT

It has been long hypothesized that topography, as well as climate and rock strength, exert first order controls on erosion rates. Here we use detrital cosmogenic ^{10}Be from 50 basins, ranging in size from 1 to 150 km^2, to measure millennial erosion rates across the San Gabriel Mountains in southern California, where a strong E–W gradient in relief compared to weak variation in precipitation and lithology allow us to isolate the relationship between topographic form and erosion rate. Our erosion rates range from 35 to 1100 m/Ma, and generally agree with both decadal sediment fluxes and long term exhumation rates inferred from low temperature thermochronometry. Catchment-mean hillslope angle increases with erosion rate until ~300 m/Ma, at which point slopes become invariant with erosion rate. Although this sort of relation has been offered as support for non-linear models of soil transport, we use 1-D analytical hillslope profiles derived from existing soil transport laws to show that a model with soil flux linear in slope, but including a slope stability threshold, is indistinguishable from a non-linear law within the scatter of our data. Catchment-mean normalized channel steepness index increases monotonically, though non-linearly, with erosion rate throughout the San Gabriel Mountains, even where catchment-mean hillslope angles have reached a threshold. This non-linearity can be mostly accounted for by a stochastic threshold incision model, though additional factors likely contribute to the observed relationship between channel steepness and erosion rate. These findings substantiate the claim that the normalized channel steepness index is an important topographic metric in active ranges.

© 2009 Elsevier B.V. All rights reserved.

1. Introduction

Modern surface topography reflects the competition and interaction between climatic and tectonic forcing. Whereas climatic and tectonic variables are often difficult to quantify, surface topography can be readily obtained for much of the Earth's land surface from spaceborne sensors and aerial photography. However, extracting quantitative understanding of the interactions among climate, topography, and tectonics requires the unraveling of the relative contributions of a complicated suite of surface processes. Consequently, a central theme in modern geomorphology involves linking surface processes and their rates to observed landforms (e.g., Dietrich et al., 2003). Such quantitative knowledge is required before we can fully exploit the archive of climatic and tectonic history that is encoded in landforms.

The importance of probing current topography for clues to process rates and mechanics is well recognized, and many have proposed that erosion rate increases with hillslope angle and local relief (e.g., Gilbert, 1877; Ahnert, 1970; Montgomery and Brandon, 2002). Basic observations support this, and the concept of slope-dependent soil flux on hillslopes has been around for over 100 years (Davis, 1892). Similarly, decadal sediment yield measurements were widely used to infer quantitative relationships between erosion rate and precipitation, uplift, and relief (e.g., Langbein and Schumm, 1958; Schumm, 1963; Judson and Ritter, 1964; Ahnert, 1970). Much uncertainty remains, however, regarding interrelationships among channel steepness, hillslope gradients, relief measured at various scales, and erosion rate even within a single climate zone. In addition, data of sufficient quality and distribution to allow rigorous testing of existing theory are sparse. Cosmogenic radionuclide (CRN) dating of surfaces and inference of erosion rates, in conjunction with the widespread availability of digital elevation models, affords an opportunity to make significant progress on this problem.

Beginning with Granger et al. (1996), there have been a number of comparisons of hillslope gradients with millennial erosion rates determined with CRN (e.g., Safran et al., 2005; Vanacker et al., 2007; Binnie et al., 2007; Stock et al., 2008; Ouimet et al., 2009), as well as studies comparing erosion rates with various measures of local relief (e.g., Burbank et al., 1996; Schaller et al., 2001; Montgomery and Brandon, 2002; Wittmann et al., 2007). As initially noted by Penck (1953) and Strahler (1950), and later recast by Burbank et al. (1996), Schmidt and Montgomery (1995), and Montgomery and Brandon (2002), meso-scale rock strength limitations result in hillslopes reaching threshold angles wherever erosion rate exceeds a critical

* Corresponding author.
E-mail address: roman.dibiase@asu.edu (R.A. DiBiase).

0012-821X/$ – see front matter © 2009 Elsevier B.V. All rights reserved.
doi:10.1016/j.epsl.2009.10.036

value. Above this rate, hillslopes are thought to respond to further increases in base level lowering rate via increasing landslide frequency (Hovius et al., 1997) and possibly slope length (Howard, 1994; Tucker and Bras, 1998). Recent studies corroborated these thoughts on the transition to threshold hillslopes and provided the first quantification of this critical erosion rate. In the semi-arid, granitic San Bernardino Mountains, Binnie et al. (2007) found that above erosion rates of ~250 m/Ma, catchment-averaged hillslope angle remains constant, consistent with field observations of landslide-dominated terrain. Ouimet et al. (2009) found similar results for semi-arid catchments in both granitic rocks and highly deformed Triassic flysch on the eastern margin of the Tibetan Plateau.

Comparison of erosion rates with channel form garnered considerably less attention, with only a few studies addressing the problem using cosmogenic radionuclides (e.g., Safran et al., 2005; Ouimet et al., 2009). Other workers (e.g., Kirby and Whipple, 2001; Lague and Davy, 2003; Snyder et al., 2003; Duvall et al., 2004) used independent measures of rock uplift rate to calibrate models of river long profile evolution. Nonetheless, there is a dearth of data suitable for quantifying many basic relationships (influence of sediment supply, climate, lithology, channel width, etc.) and for testing models of river incision into bedrock (e.g., Whipple, 2004).

In this contribution, we quantify and use CRN (^{10}Be) based erosion rates in the San Gabriel Mountains, southern California, and use a 10 m digital elevation model (DEM), to: (1) evaluate in detail different topographic metrics; (2) test the application of detrital CRN techniques to landslide-dominated catchments and across catchment sizes; (3) quantify the relationship between erosion rate and average hillslope gradient, expanding available data and evaluating existing hillslope transport models; and (4) quantify the relation between erosion rate and channel steepness and discuss implications for theory.

2. Study area

The San Gabriel Mountains (SGM) provide an excellent field setting for studying the relationship between topographic form and erosion rate. The range lies along a large restraining bend in the San Andreas Fault in southern California (Fig. 1), where active thrusting along the Sierra Madre and Cucamonga fault zones at the southern range front maintained Holocene vertical slip rate components of 0.5–0.9 mm/yr (Peterson and Wesnousky, 1994; Lindvall and Rubin, 2008). Uplift of the SGM began with the switch of activity from the San Gabriel Fault to the current trace of the San Andreas Fault, ca. 5–7 Ma (Matti and Morton, 1993). A progressive increase of dip–slip fault motion from west to east creates a strong gradient of relief, short term sediment flux (decadal reservoir fills) and long term (Myr) exhumation rates (inferred from apatite fission track and (U–Th)/He

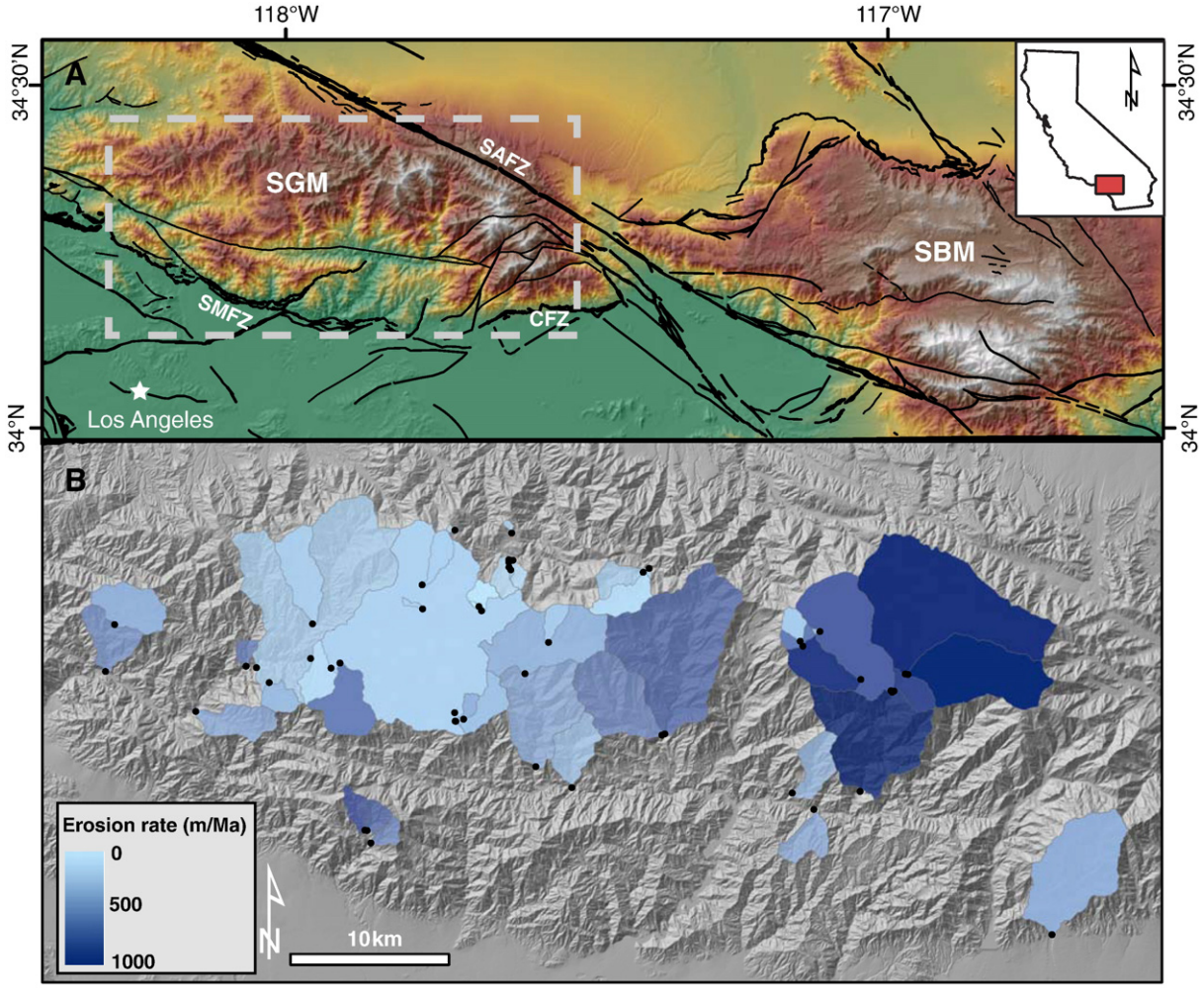

Fig. 1. (A) Overview map of central transverse ranges, CA, showing topography (0–3500 m) and quaternary faults (black lines, thickness corresponds to activity (http//earthquakes.usgs.gov/regional/qfaults/)). SGM = San Gabriel Mountains, SBM = San Bernardino Mountains, SAFZ = San Andreas Fault Zone, SMFZ = Sierra Madre Fault Zone, CFZ = Cucamonga Fault Zone. Dashed grey box indicates extent of (B), location map for basins sampled for detrital CRN (black points, polygons) in the San Gabriel Mountains. Basin color corresponds to catchment-averaged erosion rate.

thermochronology), all increasing to the east (Blythe et al., 2000; Spotila et al., 2002; Lavé and Burbank, 2004).

Mean annual precipitation rates (MAP) vary south to north, from 0.5 m/yr in the Los Angeles basin, increasing to 1.3 m/yr over the range crest, and decreasing to 0.2 m/yr in the southern Mojave Desert (PRISM — www.prism.oregonstate.edu). We focused on mainly south-draining basins with MAP ranging from 0.6 to 1.0 m/yr with elevation. The impact of this gradient on runoff is potentially mediated by a transition from rain to snow above 2000 m elevation. While detailed long-term climate is poorly constrained, there is no evidence for glaciation in the SGM.

The geology of the SGM consists primarily of Precambrian and Mesozoic granitic and metamorphic rocks. Lithological variation has two potential impacts on our analysis. First, uneven quartz distribution within basins can bias calculated basin-wide erosion rates (Bierman and Steig, 1996; Small et al., 1999). The only basin that fits this criterion, Falls Creek (SG0730), is characterized by low relief headwaters cut on a quartz-poor syenite–anorthosite complex above a major knickpoint at the lower end of the basin below which a deep gorge is cut into granite. Guided by available geologic maps (Yerkes and Campbell, 2005; Morton and Miller, 2006), all other catchment samples were carefully selected to avoid such complications. Second, material strength differences between lithologies may influence slope stability thresholds and thus catchment-mean slopes, drainage density, and relief. Similarly subtle lithologic differences could influence the fraction of sediment delivered to channels as bedload and its grain size distribution, both of which could affect the relationship between channel steepness and erosion rate. Such variations do not appear to be strong, but likely contribute to scatter in our data.

The strong E–W gradient in relief, in comparison to a weak variation in precipitation and relatively spatially homogenous lithology optimizes our ability to isolate the topographic controls on erosion. In addition, the drainage networks in the SGM are nearly fully integrated, allowing for appropriate comparisons between low and high relief landscapes across basin sizes.

We also compare our results in the SGM to a similar data set in the San Bernardino Mountains (SBM), which lie just to the east across the San Andreas Fault (Binnie et al., 2007). Lithology and climate in the SBM are similar to that of the SGM, but the topography and relief structure is strikingly different. The Big Bear Plateau dominates the central SBM, and represents an uplifted low relief surface that has yet to adjust to the regional base level (Spotila et al., 1998). Additionally, rapidly uplifting regions determined from CRN (Binnie et al., 2007) and low-temperature thermochronometry (Spotila et al., 1998; Blythe et al., 2000), are isolated and lack drainage basins larger than 10 km^2.

3. Methods

3.1. Cosmogenic erosion rates

Traditionally, erosion rates were estimated by measuring suspended sediment loads or sediment accumulation behind dams over years to decades. These methods are subject to important weaknesses; they fail to capture the role of large events, and are sensitive to anthropogenic impacts and the fire cycle (e.g., Kirchner et al., 2001; Lavé and Burbank, 2004). Catchment-averaged CRN methods, in contrast, are relatively insensitive to short term perturbations and provide geomorphically pertinent erosion rates (Bierman and Nichols, 2004; von Blanckenburg, 2005).

We measured ^{10}Be concentrations in quartz-rich sediments for 50 basins ranging in size from 1 to 150 km^2 across the region (Fig. 1) to determine catchment-averaged erosion rates (Brown et al., 1995; Granger et al., 1996; Bierman and Steig, 1996). This method has been successfully applied in numerous studies of upland landscapes (e.g., von Blanckenburg, 2005 and references within). The timescale over which the erosion rates integrate can be estimated by dividing the cosmic ray penetration depth (~0.6 m in rock) by the calculated erosion rate (for our case 0.1–1 m/ka). For the SGM, this implies timescales ranging from ~1 to 50 ka. Application of detrital CRN methods to landscapes dominated by mass wasting was evaluated numerically by Niemi et al. (2005) and Yanites et al. (2009), both of whom suggest that at high erosion rates, larger basins must be sampled to better integrate stochastic landslide inputs and to ensure adequate fluvial mixing. Field testing in the slowly-eroding Great Smoky Mountains by Matmon et al. (2003) also shows that larger basins provide more accurate measures of erosion rate. However, a recent study in the neighboring San Bernardino Mountains suggests that accurate erosion rate measurements in threshold landscapes are possible in basins as small as 1–3 km^2 (Binnie et al., 2007).

With this in mind, our sampling scheme in the SGM focused primarily on basins draining areas greater than 1 km^2 in soil-mantled catchments, and greater than 20 km^2 in bedrock dominated catchments. Large basins (>100 km^2) in both the low and high uplift regions were sampled, and we avoided catchments exhibiting strongly transient behavior (containing major knickpoints). With one exception (Cucamonga Canyon, SG162, SG163), we also avoided catchments with clear evidence of recent floods or large landslides.

For each catchment, we separated quartz using standard techniques (Kohl and Nishiizumi, 1992) while PrimeLab (Purdue University) performed the ^{10}Be isolation and measurement. We calculated ^{10}Be production rates for each catchment, correcting for elevation and latitude on a pixel by pixel basis using the 10 m DEM for the catchment (Dunai, 2000). Topographic shielding, snow cover, and muogenic production were not accounted for, and contribute to an estimated 5% uncertainty in production rates that is added to the 1σ analytical error. Although we lacked data to precisely quantify possible variability in quartz content, we do not expect significant variation as nearly all of the basins sample quartz-rich basement rocks or granitic intrusions. Comparing our data with that of Binnie et al. (2007) in the SBM (Fig. 1) enables an excellent test of the reproducibility and reliability of the detrital CRN method in rapidly eroding mountainous topography; catchments span similar ranges of topographic metrics in very similar settings, but different researchers selected sampling locations, different laboratories prepared targets, different facilities measured ^{10}Be, and our combined data encompass a wide range of catchment size across the full spectrum of erosion rates. The range of catchment sizes and the development of relations between erosion rate and topographic metrics also begin to test the model predictions that the detrital CRN method will typically underestimate erosion rates where landsliding is a common process, and that this underestimation increases with decreasing catchment size (Niemi et al., 2005; Yanites et al., 2009).

3.2. Catchment-mean hillslope angle

We used a 10 m digital elevation model to extract a catchment-mean hillslope angle for each sample basin. Local slope for each pixel in the DEM is the dip of a plane fit to a 3×3 array of pixels centered on the pixel of interest, and we averaged individual pixel slopes for each catchment. To focus our attention on the hillslopes, we selectively excluded valley fill from our calculation, though few of our sample basins are significantly aggraded. As our sampling strategy excluded transient basins characterized by prominent knickpoints, inner gorges, and remnant patches of low-relief landscapes at high elevation, calculating catchment-mean hillslope angle for SGM sample basins is straightforward.

Evaluating a representative hillslope from transient basins, in which there is a bimodal hillslope distribution is more complicated, and seven catchments used by Binnie et al. (2007) are affected. These catchments primarily lie along the southern front of the Big Bear Plateau, with this relict, low relief surface contributing significantly (20–30%) to their

catchment areas. A minimum value for the representative catchment-mean hillslope angle is simply the mean slope in the entire catchment, as reported by Binnie et al. (2007). However, as the CRN-derived erosion rate will be strongly weighted to the steep, incised lower portions of these catchments, the catchment-mean hillslope angle associated with this erosion rate is probably closer to the mean hillslope angle downstream of the plateau edge (which provides a maximum estimate of the representative catchment-mean hillslope angle). We use these minimum and maximum bounds to define error bars on catchment-mean slope and take a weighted average of these slopes as a best estimate. The mean slopes of the part of the catchment on the plateau and that below the plateau were weighted by their predicted fractional contribution to the total sediment flux out of the basin, based on the relationship between erosion rate and mean slope defined by our data in the SGM. Generally this flux-weighted mean slope is close to the maximum estimate given by the mean slope of the steep, incised lower portions of these disequilibrium catchments. We show both minimum and maximum representative catchment-mean slope in plots and stress that these points are included for visual comparison only. The complexity of these seven basins does highlight the importance of selecting well-adjusted catchments with uniform topographic characteristics to most clearly define the relationships among topographic metrics and erosion rate.

3.3. Catchment-mean channel steepness index

Graded fluvial channels tend to follow a power-law relationship between local slope (S) and upstream drainage area (A) commonly referred to as Flint's law (Hack, 1957; Flint, 1974):

$$S = k_s A^{-\theta} \tag{1}$$

where k_s is the channel steepness index and θ is the concavity index. Models of fluvial incision ranging from detachment-limited to transport-limited end-members all predict a monotonic relation between channel slope and rock uplift rate at steady state (when erosion rate = rock uplift rate), generally well approximated as a power-law relation (Snyder et al., 2003; Sklar and Dietrich, 2004; Lague et al., 2005):

$$S \propto U^p \propto k_s \tag{2}$$

The predicted relation between k_s and U varies between models and depends on climate, rock strength, and dominant incision process (e.g., plucking, bedload abrasion). For the well known end-member stream power models of detachment-limited and transport-limited incision, channel steepness index k_s is given by, respectively:

$$k_s = (U/K_d)^{1/n} \tag{3A}$$

$$k_s = (\beta U/K_t)^{1/n_t} \tag{3B}$$

where U is rock uplift rate, n and n_t are the stream power slope exponents, such that $p = 1/n$ or $1/n_t$, for detachment- and transport-limited cases, respectively, K_d and K_t are the coefficients of erosional efficiency (function of climate, lithology, etc.) for detachment- and transport-limited cases, respectively, and β is the fraction of total load delivered to channels as bedload. These and most other models predict that channel concavity is independent of rock uplift rate at steady state (e.g., Whipple and Tucker, 1999), an expectation borne out by field observations in many landscapes, including the SGM (Tucker and Whipple, 2002; Wobus et al., 2006). In analyses of topographic data using Eq. (1), a complication arises in that slight variations in best-fit concavity index (θ) exist in every landscape and estimates of k_s are strongly correlated to the fit concavity index (e.g., Sklar and Dietrich, 1998). This can be resolved by evaluating a normalized channel steepness index using a fixed reference concavity, θ_{ref} (e.g., Wobus et al., 2006):

$$S = k_{sn} A^{-\theta_{ref}} \tag{4}$$

By fixing $\theta = \theta_{ref}$, and making the assumption that K_d and n do not vary systematically across the landscape, k_{sn} (normalized channel steepness index) proves to be a useful metric for studying the relations between topography and rock uplift or erosion (e.g. Snyder et al., 2000; Kirby and Whipple, 2001; Kobor and Roering, 2004; Hilley and Arrowsmith, 2008). Wobus et al. (2006) provide additional examples and detailed methodology concerning the extraction of river profile topography from DEMs and the fitting of k_{sn} to individual channel segments.

For this study, we determined a representative k_{sn} for each of our sample basins in the SGM, and also where possible (i.e., for catchments of sufficient size) for the basins sampled in the SBM by Binnie et al. (2007). We followed a methodology similar to that used by Ouimet et al. (2009). Using a fixed reference concavity index of 0.45, we used a freely available set of Matlab and ArcMap scripts (http://www.geomorphtools.org) to automate profile fits for all channel reaches (500 m segments) draining >2 km^2 from the 10 m resolution USGS NED DEM (Fig. 2). We report the catchment average k_{sn} for each sample basin as the mean k_{sn} of all individual reaches, with an uncertainty of 2 standard errors about this mean. Errors associated with individual reach fits (2 standard deviations) are much less than intra-basin variability of k_{sn}. We did not assign a channel steepness index to small (<3 km^2), steep, rocky catchments (especially those in the SBM), as the slope-area data for these basins do not conform to Flint's law, showing little or no variation of slope with drainage area.

3.4. Catchment-mean local relief

Studies of the controls on denudation rate often use various measures of topographic relief as their primary topographic metric (e.g., Ahnert, 1970; Montgomery and Brandon, 2002; Aalto et al., 2006). Relief is by definition a scale-dependent measurement, and how the scale of analysis affects what aspect of topographic form (hillslope relief, colluvial channel relief, fluvial tributary relief, main stem relief, and combinations thereof) is measured has never been systematically evaluated. Here we quantify the relations among mean hillslope angle, mean channel steepness index, and mean local relief measured over a wide range of length scales for all the catchments sampled within the SGM. Following Ahnert (1970) and Montgomery and Brandon (2002), for each pixel in the SGM DEM we measured local relief within a circular window with radius ranging from 100 m to 5 km. Catchment-mean local relief is simply the average of all values within a catchment. It should be noted that for small catchments and large relief windows, local relief calculations may incorporate topography outside of the basin. For convenience we plot these data as normalized mean local relief, where normalized local relief is defined as elevation range divided by window diameter.

4. Results

4.1. Interrelations among topographic metrics

Catchment-mean hillslope angle increases with increasing channel steepness index until $k_{sn} \sim 100\ m^{0.9}$, above which hillslope angles become invariant (Fig. 3). The form of this relationship supports the hypothesis that channel steepness reflects erosion rates, thus retaining a tectonic signature, in landscapes where hillslopes have achieved threshold gradients, and corroborates the similar relationship found by Ouimet et al. (2009).

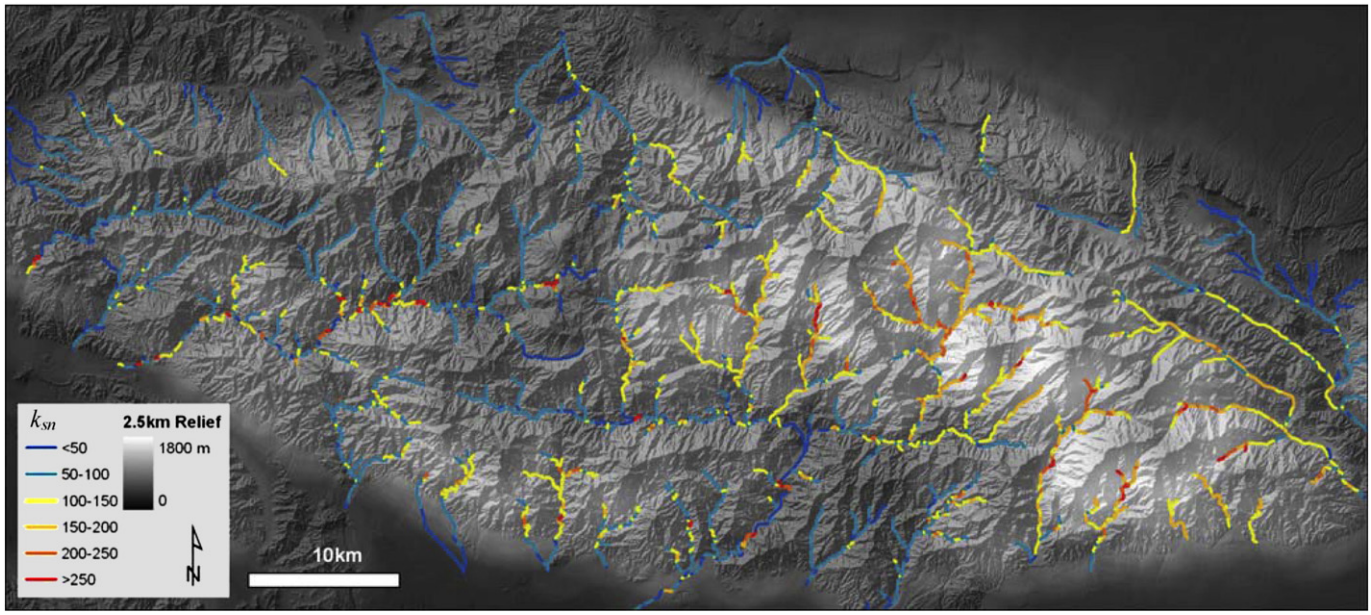

Fig. 2. Map of normalized channel steepness index (k_{sn}) draped on top of 2.5 km relief in the San Gabriel Mountains. Although there is a direct correlation between the two, channel profiles contain additional high resolution information about both spatial and temporal patterns of uplift.

Fig. 4 highlights the complex relationships among the various topographic metrics (e.g., slope angle, relief, k_{sn}), and the significant influence of the measurement scale of relief. At the smallest scales (10s to 100s of m) local relief is simply a proxy for hillslope angle. Indeed, hillslope gradient can be thought of as fine scale relief normalized for the length scale over which it is measured. Relief measured with a 100 m radius window is tightly correlated to mean basin gradient (Fig. 4A), while at progressively larger scales (1–5 km), tributary channel relief begins to dwarf hillslope relief (Whipple et al., 1999), and local relief begins to be a measure of tributary channel steepness. At still larger scales (>10 km) trunk channel relief is incorporated, and eventually relief becomes solely a measure of range height. In the SGM, relief measured with a 2.5 km radius window tracks linearly with channel steepness index (Fig. 4B). In addition, the spatial pattern of 2.5 km-scale local relief maps directly with the spatial pattern of channel steepness index values (Fig. 2). This optimal relief scale is not universal and can be expected to vary with catchment size, relief magnitude, and drainage density.

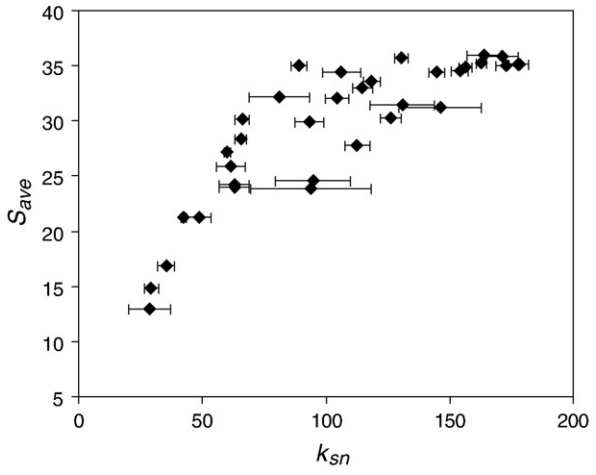

Fig. 3. Catchment-averaged slope (S_{ave}) vs. normalized channel steepness index (k_{sn}) for SGM sample basins.

Though these two metrics are strongly correlated, there are important advantages to using k_{sn} rather than relief. First, not all of the spatial variation in channel steepness is captured by km-scale relief; lithologic controls on channel steepness, uplift patterns associated with active structures, and knickpoints associated with accelerated incision are much more finely resolved using k_{sn}. Additionally, k_{sn} can be derived from specific, process-based models of river incision and is scale independent, while local relief always measures a combination of landscape elements (e.g., hillslope relief, colluvial and fluvial channel steepness, channel length) governed by distinct processes and involves additional uncertainty in determining an appropriate measurement scale. Relief is however, easier and quicker to calculate than channel steepness, and can yield information in preliminary landscape analysis to help direct further, more detailed topographic examination.

4.2. Spatial distribution of topographic metrics

Catchment-mean hillslope angle in the SGM varies from 10 to 38°, generally increasing from west to east until hillslopes attain threshold values. No clear dependence of catchment-mean slope on drainage area is seen. Basin slope distributions are predominantly normally distributed; skewed or bimodal distributions are either attributable to large areas of low slope such as wide valley bottoms and terraces or reflect potential disequilibrium conditions with low relief surfaces perched above significant knickpoints in channel profiles.

Local channel steepness values range from below 20 to over 500 $m^{0.9}$ (Fig. 2). However, the highest values are confined primarily to immediately below significant knickpoints. Catchment-mean k_{sn} in the SGM ranges from 20 to 200 $m^{0.9}$, covering much of the known worldwide variation in k_{sn} (Wobus et al., 2006). Similar to hillslope angle, channel steepness index increases generally from west to east, with no dependence on drainage area. Basins from the SBM sampled by Binnie et al. (2007) for detrital CRN were also analyzed for comparison. In the SBM, channel steepness index averaged over the basin has a smaller range than in the SGM. This likely reflects the fact that all of the rapidly eroding (>0.7 mm/yr) SBM sample basins are less than 2 km^2. These channels likely are entirely dominated by debris flows (e.g., Montgomery and Foufoula-Georgiou, 1993; Stock and Dietrich, 2003), making determination of channel steepness values inappropriate.

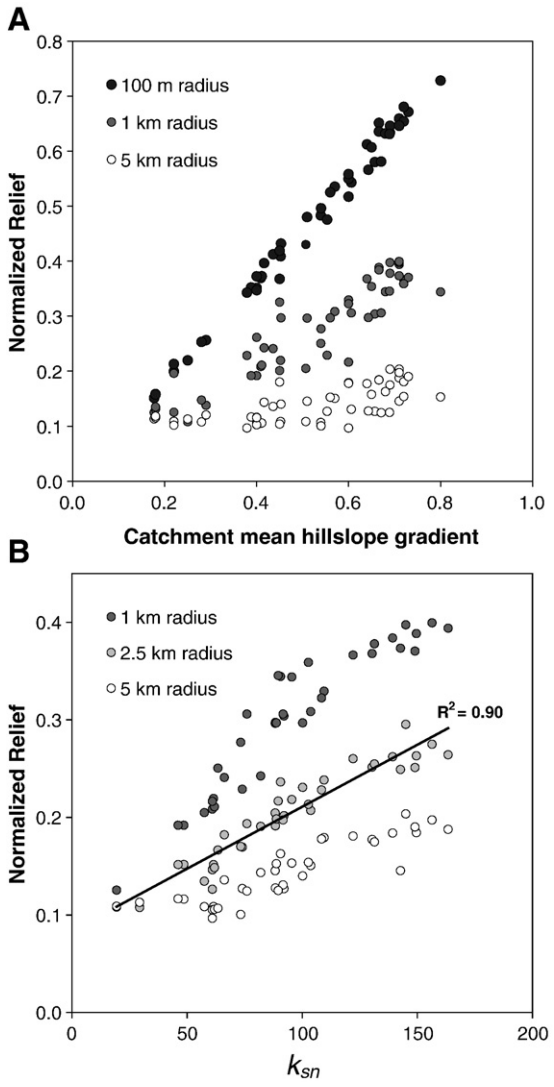

Fig. 4. (A) Measured at 100 m scale, local relief is nearly identical to hillslope angle, but as the scale of relief measurement increases, both the scatter and non-linearity of the relief-hillslope angle relationship increase. (B) At a radius of 2.5 km, relief increases linearly with channel steepness. Measured at 1 km scale or less, relief values reach a threshold similar to that shown in Fig. 3. Large scales of relief smooth out the variability that we are interested in from the landscape.

4.3. Erosion rates and topography

Catchment-averaged erosion rates, inferred from ^{10}Be concentrations in alluvial sands, range from 35 to 1100 m/Ma in the SGM (Table 1), and are in general agreement with both long-term (Ma) estimates from low-temperature thermochronometry work (Blythe et al., 2000; Spotila et al., 2002) and decadal sediment yield data compiled by Lavé and Burbank (2004). For catchments sampled in the SGM, we do not expect the actual erosion rates to have any dependence on drainage area. However, for reasons discussed earlier, we expect that the CRN-derived erosion rates may systematically underestimate the actual erosion rates for landslide-dominated catchments, with the effect being strongest for small catchments (<10 km^2) (Niemi et al., 2005; Yanites et al., 2009). Although we introduced a slight sampling bias towards larger basins in areas of high relief to account for this effect, our measured erosion rates in the SGM show little dependence on drainage area across a wide range of both basin size (0.1–100 km^2) and erosion rate (10–1000 m/Ma, Fig. 5). In addition, in the SBM, rapid uplift is constrained to narrow ridges between faults that preclude sampling large, high relief basins. As a result, there is a sampling bias towards smaller basins at high erosion rates (Binnie et al., 2007). Taken together, there appears to be no dependence of CRN-derived erosion rate on drainage area, though it should be noted that neither of these two datasets were collected with the explicit intention of testing this hypothesis. The data suggest that models of the impact of stochastic sediment delivery on erosion rates estimated from detrital CRN concentrations may exaggerate the influence of large landslides, a tentative conclusion that warrants caution applying these models for data interpretation and merits further investigation.

Catchment-mean hillslope angle increases with erosion rate until ~300 m/Ma (Fig. 6). At erosion rates higher than ~300 m/Ma, catchment-averaged slopes are invariant at a threshold value of ~35°. Detrital CRN data from the SBM (Binnie et al., 2007) are also plotted here and follow the same trend, particularly after correcting mean slope estimates for SBM basins with headwater reaches on the Big Bear plateau surface.

Channel steepness index increases non-linearly but monotonically with erosion rate throughout the range of observed erosion rates, with some scatter (Fig. 7). The channel steepness index therefore records erosion rate information in threshold landscapes, where hillslope form is no longer sensitive to erosion rate, and thus serves as a key metric for interpreting rapidly eroding landscapes in tectonically active settings (see also Ouimet et al., 2009). Comparison with channel profile analysis of the SBM dataset shows a very similar trend for erosion rates below 500 m/Ma. As noted earlier, more rapidly eroding basins in the SBM are almost all too small to allow meaningful assessment of the normalized channel steepness index.

5. Analysis

5.1. Catchment-mean slope and erosion rate

To model the morphological transition from slope-dependent to threshold hillslopes, soil transport laws that account for both creep-related and landslide processes must be used (e.g., Howard, 1994; Anderson, 1994; Roering et al., 1999). Two end-member approaches allow for analytical 1-D profile analysis:

$$q_s = \frac{-KS}{1-(S/S_c)^2} \tag{5A}$$

$$\begin{aligned} q_s &= -KS; \quad |S|<S_c \\ q_s &= \infty; \quad\quad |S|\geq S_c \end{aligned} \tag{5B}$$

where q_s is the volumetric soil flux (m^2/yr), K is the transport coefficient (m^2/yr), S is local slope (dz/dx), and S_c is a critical slope at which soil flux approaches infinity. Eq. (5A) is a non-linear transport law (Roering et al., 1999) supported by field (e.g., Pelletier and Cline, 2007) and experimental (e.g., Gabet, 2003) studies, while Eq. (5B) represents a simple, linear slope-dependent flux at slopes less than critical, with a transition to infinite potential soil transport capacity above a threshold slope. Both of these models can be combined with a statement of mass conservation to derive one-dimensional steady-state characteristic forms (e.g., Kirkby, 1971; Roering et al., 2007):

$$z(x) = \frac{KS_c^2}{2(\rho_r/\rho_s)E}\left[\ln\left(\frac{1}{2}\left(\sqrt{1+\left(\frac{2(\rho_r/\rho_s)Ex}{KS_c}\right)^2}+1\right)\right)-\sqrt{1+\left(\frac{2(\rho_r/\rho_s)Ex}{KS_c}\right)^2}+1\right] \tag{6A}$$

$$\begin{aligned} z(x) &= \frac{-(\rho_r/\rho_s)Ex^2}{2K} \quad x<x_t \\ z(x) &= -S_c x + \frac{1}{2}S_c x_t \quad x\geq x_t \end{aligned} \tag{6B}$$

$$x_t = \frac{KS_c}{(\rho_r/\rho_s)E}$$

Table 1
Detrital CRN sample basin location, morphometry and erosion rate data.

Sample ID	Easting [a]	Northing [a]	Area (km^2)	Mean elevation (m)	Basin relief (m)	S_{ave} (°)	k_{sn}	$^{10}Be/SiO_2$ ($\times 10^3$ atoms/g)	N(z,I) [b]	Erosion rate (m/Ma) [c]
SGB1	393590	3796490	174.70	1401	1438	25.9	62 ± 6	73.21 ± 14.6	2.46	109 ± 27
SGB2	398070	3796470	102.00	1448	1200	24.2	63 ± 6	69.03 ± 17.25	2.54	119 ± 36
SGB3	396850	3797050	106.90	1437	1268	24.0	63 ± 6	96.74 ± 13.99	2.52	84 ± 16
SGB4	405576	3793270	6.00	1528	489	21.3	43 ± 1	244.33 ± 243.44	2.67	35 ± 37
SGB5	396964	3799133	9.91	1358	817	27.2	60 ± 1	56.53 ± 10.86	2.37	135 ± 33
SGB6	385052	3799080	9.68	1286	875	33.0	115 ± 4	29.39 ± 12.46	2.23	246 ± 117
SGB7	394360	3795594	3.18	1311	770	34.4	106 ± 8	29.16 ± 4.74	2.27	253 ± 54
SGB9	384501	3796261	17.33	1139	1189	33.6	118 ± 3	15.33 ± 0.56	2.01	424 ± 37
SGB10	389930	3793860	7.48	1107	1042	32.1	105 ± 5	22.56 ± 0.76	1.94	279 ± 23
SGB11	431950	3795090	82.45	1953	2131	34.9	157 ± 3	14.82 ± 0.67	3.78	826 ± 79
SGB12	429900	3789052	148.38	1803	2463	35.3	163 ± 2	11.07 ± 0.63	3.45	1010 ± 108
SGB13	431750	3795109	35.03	1959	1921	35.2	178 ± 4	28.22 ± 1.84	3.80	436 ± 50
SG116	406050	3793401	1.11	1511	400	22.5	N/A	27.15 ± 2.54	2.64	314 ± 45
SG118	405531	3793280	6.03	1527	494	21.2	43 ± 1	2.57 ± 2.25	2.67	265 ± 32
SG123	403550	3801480	3.19	1731	838	28.4	66 ± 2	93.68 ± 3.95	3.14	108 ± 10
SG124	403580	3800022	0.35	1409	445	24.2	N/A	52.55 ± 3.06	2.44	151 ± 16
SG125	400471	3785950	1.96	1336	858	33.6	N/A	16.14 ± 1.32	2.32	465 ± 61
SG126	400230	3786700	2.30	1361	801	36.4	N/A	12.94 ± 0.9	2.36	591 ± 71
SG127	400100	3786719	2.60	1344	934	39.1	N/A	10.26 ± 0.87	2.33	736 ± 99
SG128	407130	3799908	2.13	1790	182	12.9	29 ± 8	250.69 ± 20.68	3.25	42 ± 6
SG129	406977	3800170	0.14	1788	149	16.0	N/A	213.83 ± 57.3	3.24	49 ± 16
SG130	408940	3804594	0.29	1734	230	25.5	N/A	138.47 ± 9.04	3.12	73 ± 8
SG131	408762	3802978	2.30	1738	250	14.9	29 ± 3	102.88 ± 12.7	3.13	98 ± 17
SG132	409009	3802950	1.13	1728	257	16.8	35 ± 4	94.48 ± 4.54	3.10	106 ± 10
SG136	427489	3798670	0.11	2275	203	24.4	N/A	103.09 ± 4.45	4.60	144 ± 13
SG137	418150	3792511	46.84	1524	1863	34.6	154 ± 3	15.05 ± 1.4	2.75	591 ± 84
SG138	417980	3792440	17.88	1383	1699	35.7	131 ± 3	18.65 ± 2.75	2.47	428 ± 85
SG140	412561	3789280	7.71	1071	1044	29.9	93 ± 6	32.49 ± 1.99	1.89	189 ± 21
SG141	410390	3790543	43.06	1526	1696	30.2	126 ± 4	30.45 ± 2.38	2.74	292 ± 37
SG150	405510	3793789	0.02	1378	56	13.3	N/A	23.82 ± 2.57	2.38	323 ± 51
SG151	426461	3797780	3.53	2290	813	31.2	146 ± 17	34.82 ± 10.27	4.67	434 ± 150
SG152	426300	3798089	2.10	2343	738	31.4	N/A	199.29 ± 9.52	4.85	79 ± 8
SG157	432789	3796090	25.39	2019	2046	35.0	173 ± 5	11.68 ± 1.57	3.99	1106 ± 204
SG158	432614	3796111	53.21	1949	1922	34.4	145 ± 3	11.68 ± 1.39	3.75	1039 ± 175
SG159	431831	3795020	35.03	1958	1929	35.2	178 ± 4	17.15 ± 1.67	3.80	717 ± 106
SG161	429939	3795791	11.55	1954	1550	36.0	164 ± 7	12.03 ± 1.69	3.74	1006 ± 191
SG162	441441	3780431	27.99	1570	2036	35.9	172 ± 6	33.69 ± 4.63	2.91	279 ± 52
SG163	441440	3780432	27.99	1570	2036	35.9	172 ± 6	43.13 ± 2.83	2.91	218 ± 25
SG204	408889	3802380	0.08	1706	73	10.2	N/A	16 ± 2.18	3.05	617 ± 115
SG205	408780	3802535	0.12	1697	90	10.6	N/A	89.34 ± 5.77	3.03	110 ± 13
SG206	427120	3787967	5.39	862	632	32.2	81 ± 12	18.56 ± 5.21	1.59	277 ± 91
SG207	425810	3788950	6.52	1053	1254	35.1	89 ± 3	23.04 ± 2.33	1.89	265 ± 40
SG0701	408768	3802844	0.19	1680	113	10.3	N/A	81.27 ± 3.49	2.99	119 ± 11
SG0702	405524	3804763	0.18	2087	179	20.8	N/A	167.58 ± 8.31	4.03	78 ± 8
SG0703	398617	3796775	9.89	1349	880	30.1	66 ± 3	12.54 ± 0.83	2.34	605 ± 70
SG0728	417222	3802455	9.07	2088	734	24.6	95 ± 15	110.91 ± 6.08	4.05	118 ± 12
SG0729	416848	3802226	5.34	2127	685	23.9	94 ± 24	155.05 ± 7.65	4.16	87 ± 9
SG0730	393010	3706541	5.69	1174	904	31.5	131 ± 13	11.55 ± 2.64	1.76	492 ± 137
SG0740	411172	3798020	2.09	1916	907	24.4	N/A	78.64 ± 4.28	3.58	147 ± 15
SG0743	409731	3796134	21.96	1725	1291	27.8	113 ± 5	42.7 ± 2.89	3.16	239 ± 28

[a] UTM coordinates (NAD 27 Datum).
[b] Production rate latitude/elevation scaling factor (Dunai, 2000).
[c] Erosion rates calculated using density of 2.6 g/cm^3, attenuation length of 165 g/cm^2, and high latitude production rate of 5.1 atoms/g/yr.

where $z(x)$ is the surface elevation, E is erosion rate, and x_t is the transition point from convex to planar hillslopes for the linear with threshold model (for full derivations of Eqs. (6A) and (7A), see Roering et al. (2007)). Taking the derivative of Eq. (6) with respect to x and averaging slope over the horizontal hillslope length L_H, steady-state relationships between profile-averaged hillslope gradient, S_{ave}, and the variables E, S_c, K, and L_H can be derived:

$$S_{ave} = S_c \frac{1}{E^*}\left(\sqrt{1+(E^*)^2} - \ln\left(\frac{1}{2}\left(1+\sqrt{1+(E^*)^2}\right)\right) - 1\right) \quad (7A)$$

$$S_{ave} = S_c\left(1-\frac{1}{E^*}\right) \quad E^* \geq 2$$
$$S_{ave} = \frac{E^* S_c}{4} \quad E^* < 2 \quad (7B)$$
$$E^* = \frac{2E(\rho_r/\rho_s)L_H}{KS_c}$$

where E^* is a dimensionless erosion rate (Roering et al., 2007). Thus for each model the average slope of a 1-D hillslope varies with K/L_H — any change to this ratio has an equivalent effect on mean slope. Note that the linear transport law with a threshold predicts a distinctly non-linear relationship between mean slope and erosion rate. Thus an observation of such a non-linear relation does not necessarily support a non-linear diffusion model. The relations between mean slope and erosion rate derived above are distinct from that proposed by Montgomery and Brandon (2002). They predict similar non-linear forms, but make explicit how measurable hillslope transport coefficients (K), hillslope length (L_H), and soil density (ρ_r/ρ_s) influence the erosion coefficient in the Montgomery and Brandon (2002) relationship.

Modeling one-dimensional hillslope profiles using the above framework is straightforward, though extending known controls on mean slope of these "characteristic forms" to full landscapes is not. Local variables that govern sediment transport (i.e., slope) must be related to basin-averaged measurements to make comparisons with catchment-

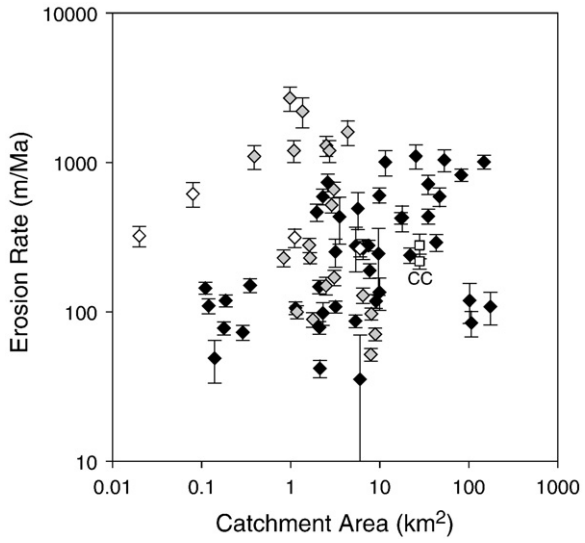

Fig. 5. CRN-derived erosion rate vs. catchment area for SGM data (black diamonds) and SBM data (Binnie et al., 2007, grey diamonds). SGM error bars include 1σ analytical error as well as an additional 5% uncertainty in ^{10}Be production rate calculation. White diamonds indicate SGM samples that are either repeats of or nested within catchments showing erosion rates less than 110 m/Ma. White squares represent Cucamonga Canyon (CC; SG162, SG163).

averaged cosmogenic erosion rates. Roering et al. (2007) have shown that, to first order, this can be done by calculating the average slope over a representative (average length, L_H) 1-D hillslope profile and equating this to the catchment-mean hillslope angle. Because this approach allows only a first order comparison, we do not attempt to use our data to constrain statistical best-fit model parameters. Instead, we aim to evaluate whether realistic values of model parameters reasonably predict observed relations between topography and erosion rates and to determine whether the two models can be distinguished based on these types of data.

Reasonable estimates of all parameter values for these hillslope soil transport models can be readily determined. Our DEM analysis suggests that $S_c \geq 35°$, consistent with estimates elsewhere (e.g., Roering et al., 2007). DEM analysis and aerial photograph interpretation suggest $L_H = 75$ m is reasonable for the SGM, but is variable within catchments and may vary with erosion rate — a complication that merits further investigation. A value of 2 is taken as the typical density ratio for granitic soils. Given these constraints, and the scatter in our data, we find that reasonable values of K (0.008 and 0.015 m^2/yr for Eq. (7A) and (7B), respectively) and S_c (39° and 37° for Eq. (7A) and (7B), respectively) provide visually satisfying fits to our data using both models (solid lines in Fig. 6). In addition to inherent uncertainty in erosion rate estimates from detrital CRN concentrations, scatter in our data is likely due to variability in lithology, hillslope length, and aspect within our sample basins, and should be expected with such a crude mapping of the local, process-controlling slope to a variable such as catchment-mean hillslope angle.

5.2. Catchment-mean channel steepness index and erosion rate

As noted earlier, channel steepness index increases non-linearly with erosion rate in the SGM, and approximately follows the power-law relation described by Eq. (2) where $p \sim 1/2$. Other researchers have found this relationship to be approximately described by $p = 1$ (Kirby and Whipple, 2001; Lague and Davy, 2003), $p = 1/2$ (Ouimet et al., 2009), and $p = 1/4$ (Snyder et al., 2003). The stream power model of detachment-limited bedrock incision is consistent with a range of non-linear behaviors ($3/5 \leq p \leq 3/2$), depending on process mechanics (Hancock et al., 1998; Whipple et al., 2000). However, for $p < 1$ channels are predicted to become buried in sediment as erosion rates and sediment fluxes increase such that they are forced to maintain a slope sufficient to transport the full sediment load (Tucker and Whipple, 2002). Consistent with this, the majority of channels in the SGM, including those in high relief, rapidly eroding areas, show little bedrock exposure in their beds and are likely transporting sediment near capacity. Simple models (e.g., Eq. (3B)) for this transport-limited condition predict $p = 1$ (bedload transport capacity is linear in slope), implying $p \geq 1$ across the SGM.

In light of the expectation that a transition to transport-limited conditions will preclude a sub-linear relationship between channel steepness and erosion rate, why our data suggest $p = ½$ becomes an important question. To account for the observed non-linear relationship between channel steepness and erosion rate ($p < 1$), transport as well as detachment processes must be affected. We use here the stochastic threshold model of Tucker and Bras (2000) and Tucker

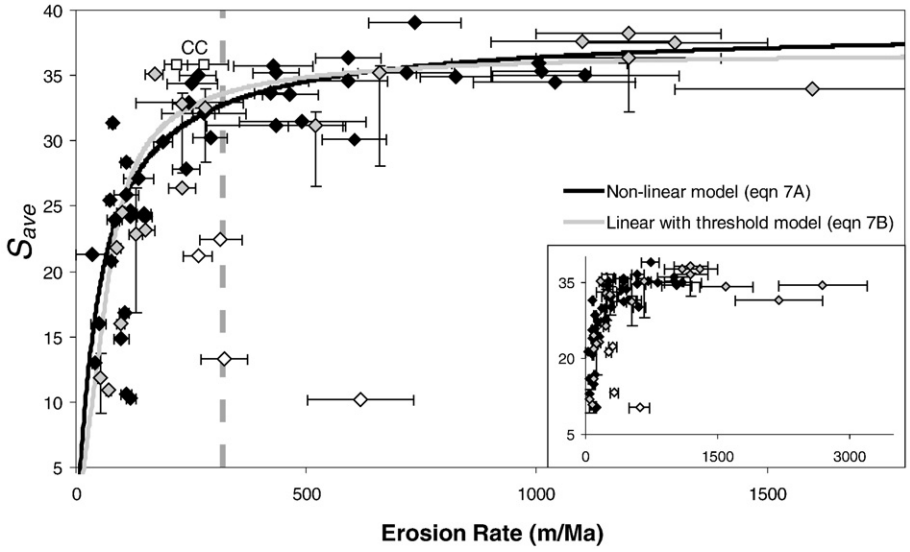

Fig. 6. Catchment average hillslope angle (S_{ave}) vs. CRN-derived erosion rate (symbols as in Fig. 5). Inset plot shows full range of SBM data. Non-linear model shown with $S_c = 39°$, $K = 0.008$ m^2/yr, $L_H = 75$ m. Linear with threshold model shown with $S_c = 37°$, $K = 0.015$ m^2/yr, and $L_H = 75$ m. Dashed grey line indicates maximum surface soil production rate measured in the SGM from Heimsath (1999).

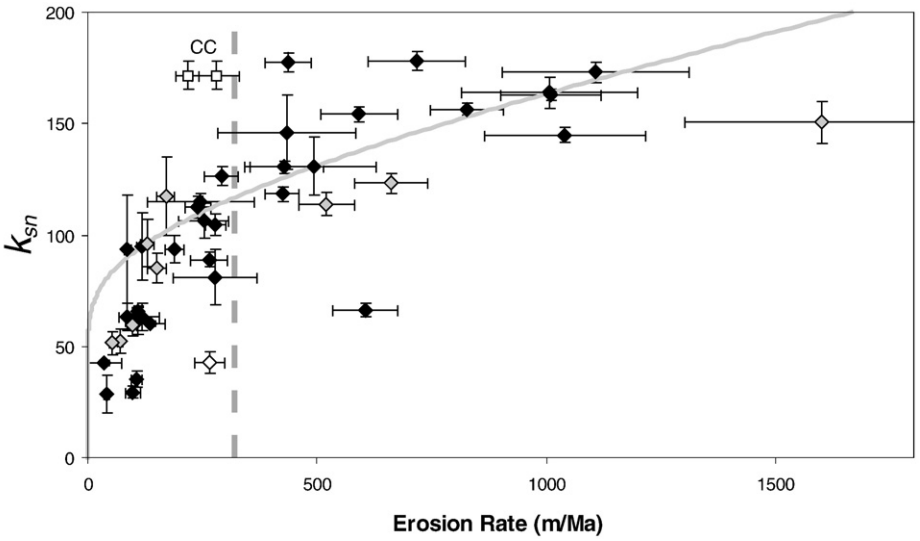

Fig. 7. Catchment-mean normalized channel steepness index vs. CRN-derived erosion rate (symbols as in Fig. 5). Data shown only for basins draining >2 km^2 (47 out of 70 basins). Grey line shows result of stochastic threshold model with the following parameters: mean rainfall intensity = 3 mm/h, mean storm duration = 7 h, mean interstorm period = 238 h, threshold shear stress τ_c = 55 Pa (equivalent to movement of 11 cm cobbles), and erosional efficiency k_e = 0.0003 (see Tucker, 2004 for full explanations of variables). Dashed grey line indicates maximum surface soil production rate measured in the SGM from Heimsath (1999).

(2004), which combines a threshold shear stress for motion or detachment with variable discharge via an exponential probability distribution of rainfall in a stream power type incision model.

In its simplest form, the stochastic threshold model expands the coefficient of erosional efficiency, K_d in Eq. (3A), into three terms, such that:

$$E = K_R K_C K_{\tau c} A^m S^n \tag{8}$$

where K_R encompasses the physical parameters of channel geometry, hydraulic roughness, and substrate resistance to erosion, K_C is a function of stochastic climate parameters, and $K_{\tau c}$ is a threshold term set by the critical shear stress and local channel slope that varies between 0 and 1 (Whipple, 2004; Tucker, 2004). To illustrate the implications of this model for the SGM data, we used channel geometry and hydraulic roughness constants consistent with Snyder et al. (2003) and Tucker (2004). Climate parameters were estimated from rainfall records at Mt. Baldy (National Climatic Data Center — http://www.ncdc.noaa.gov), and kept constant for all basins. We then adjusted the critical shear stress (controls height of rollover) and substrate resistance to erosion (controls slope of curve at high erosion rate) to fit our data by eye in Fig. 7. We find that the stochastic threshold model can explain much of the variance in our data using reasonable parameter estimates (Fig. 7).

6. Discussion

6.1. Implications for channel incision theory

Our analysis demonstrates that much of the non-linearity of the relation between channel steepness index and erosion rate (p<1) can be explained by the combined effects of a critical threshold for bedload entrainment or bedrock detachment and a stochastic distribution of floods (Fig. 7). This is, however, a non-unique finding. There are numerous alternate mechanisms for generating p<1. Two frequently discussed factors include orographic precipitation effects (Roe et al., 2002), and a narrowing of channel width with erosion rate (Finnegan et al., 2005), but neither appear to play an important role in the SGM. We purposefully selected catchments with only weak orographic effects (mean annual rainfall increases from ~0.6 to ~0.9 m/yr from low to high relief catchments). Also, field observations do not support significant channel narrowing with increased erosion rate in well-adjusted, quasi-equilibrium catchments (DiBiase et al., 2007). In addition, systematic changes in the caliber, durability, and fraction of bedload sediment (β) with erosion rate, as well as an increase in debris flow activity with increasing erosion rate, may influence the relationship between k_{sn} and erosion rate (e.g., Stock and Dietrich, 2003; Sklar and Dietrich, 2006). Additional field measurements are necessary to evaluate how important these factors may be in this, and other, landscapes.

What is most satisfying about the simple stochastic threshold model illustrated in Fig. 7 is that it incorporates only effects that we know with certainty must operate in all landscapes (thresholds of motion and/or detachment and stochastic floods). Much of the non-linearity in the relation between channel steepness index and erosion rate seen in our data can be explained by these effects alone, suggesting that, in aggregate, other factors exert only a secondary influence. Additional erosion rate and topography data from a range of landscapes in different geologic, tectonic, and climatic settings will be required to fully evaluate this tentative conclusion.

6.2. Implications for hillslope transport theory

A non-linear relation between catchment-mean hillslope angle and erosion rate is used (e.g., Montgomery and Brandon, 2002; Roering et al., 2007) to support the non-linear transport model of Roering et al. (1999). Whereas available data is consistent with this model, our analysis demonstrates that the simpler linear-threshold model (Eq. (7B)) fits the data from the SGM and SBM equally well. Indeed, predictions of the two models are so similar that they will likely remain indistinguishable on the basis of the relation between mean slope and erosion rate, though experimental studies of granular creep (Roering et al., 2001) and dry ravel (Gabet, 2003) clearly distinguish and support the non-linear model. Ouimet et al. (2009) reached a similar conclusion based on their data from catchments on the eastern margin of the Tibetan Plateau (ETP).

Interestingly, very similar values of the hillslope transport coefficient (K) provide the visually most satisfying fit to data from SGM/SBM (~−0.008 m^2/yr) and the ETP (~0.006 m^2/yr) (Ouimet et al., 2009), consistent with more direct estimates of K in many semi-arid to temperate landscapes (e.g., Hanks et al., 1984). Moreover, although the SGM/SBM data require a higher threshold slope (S_c~38°

vs. ~32° for the ETP dataset), this merely reflects the difference in DEM resolution available in the two regions (10 m in SGM/SBM vs. 90 m in the ETP) (Ouimet et al., 2009). It is tempting to speculate that these hillslope transport model parameters may be insensitive to geologic and climatic conditions. However, both field sites are semi-arid, and the ETP data includes a significant fraction of catchments underlain by granitic rocks. Similar field data is needed from field sites spanning a range of geologic and climatic conditions before any firm conclusions can be drawn. Nonetheless, it is remarkable that no distinction can be made either between the SGM/SBM and the ETP datasets or between catchments underlain by granitic rocks and highly deformed Triassic flysch within the ETP dataset (Ouimet et al., 2009).

The transition to slope-invariant erosion rates above ~300 m/Ma is interpreted to represent a change from steady, creep-related processes (e.g. tree throw, burrowing) to mass wasting and the achievement of threshold slopes (e.g., Montgomery and Brandon, 2002; Binnie et al., 2007; Ouimet et al., 2009). Field observations in the SGM are consistent with this interpretation. At low erosion rates (<150 m/Ma), basins are nearly entirely mantled by a thin (<1 m) layer of mobile, well-mixed soil and hilltops are smoothly convex up. In rapidly eroding basins (>400 m/Ma), the soil mantle has been mostly replaced with a patchwork of talus, bare bedrock, and landslide scarps and deposits on roughly planar slopes with rugged ridgelines.

Cosmogenically determined soil production rates typically show an inverse exponential relationship with soil depth (e.g., Heimsath et al., 1997; 2005). In these studies, the maximum surface soil production rates range from ~50 to 250 m/Ma, and the transition to threshold slopes is thought to correspond to erosion exceeding these rates. Soil production rates measured in the SGM reach a maximum of either 100 or 300 m/Ma, depending on locality, closely matching the erosion rate responsible for the development of threshold hillslopes (Heimsath, 1999; DiBiase et al., 2008). This represents the first quantitative test of the hypothesis that the transition to threshold hillslopes corresponds to erosion exceeding the 'speed limit' set by the conversion of bedrock to soil. Further work is needed to test whether this speed limit varies with uplift rate; the coupling of chemical weathering with physical erosion rate may complicate this first cut interpretation.

7. Conclusions

The location of the San Gabriel Mountains along a restraining bend in the San Andreas Fault sets up a strong gradient of tectonic forcing (and relief) over a relatively small (100×30 km) region with minimally varying climate and lithology. Catchment-mean hillslope angle, channel steepness index, and local relief measured at various scales all increase from west to east. We measured ^{10}Be concentrations in 50 alluvial sand samples to determine catchment-averaged, millennial scale erosion rates across the range. These rates show little dependence on drainage area (which ranges from 0.1 to 100 km^2 in our dataset), in contrast to expectations from numerical experiments (Niemi et al., 2005; Yanites et al., 2009), suggesting that steep basins as small as 1–3 km^2 yield accurate detrital CRN erosion rates. Catchment-mean hillslope angle increases with erosion rate until ~300 m/Ma, above which slopes become invariant with erosion rate. This transition in form is seen both in the field, as a switch from soil-mantled to bedrock landscapes, and in local soil production rates, which suggest a maximum bedrock weathering rate of 100–300 m/Ma (Heimsath, 1999; DiBiase et al., 2008). Similar data has supported a non-linear soil transport law (e.g., Montgomery and Brandon, 2002), but we show that a simpler linear with threshold hillslope transport law fits our data equally well. Normalized channel steepness index tracks monotonically, though non-linearly, with erosion rate throughout the SGM. Much of this non-linearity can be ascribed to the addition of a threshold shear stress and variable discharge to the stream power models of either detachment- or transport-limited river incision. Normalized channel steepness thus serves as a reliable topographic metric of erosion rate in actively deforming orogens where threshold hillslopes fail to retain a tectonic signature.

Acknowledgements

Many thanks are due to those involved with collecting samples and assisting with field work, especially the MIT field classes led by KXW in 2002 and KXW and AMH in 2006. Two anonymous reviewers helped improve the manuscript. This work was supported by funding from the Geomorphology and Landuse Dynamics Program at NSF (EAR-0724194 to KXW, EAR-0518998 to AMH).

References

Aalto, R., Dunne, T., Guyot, J.L., 2006. Geomorphic controls on Andean denudation rates. J. Geol. 114, 85–99.
Ahnert, F., 1970. Functional relationships between denudation, relief, and uplift in large mid-latitude drainage basins. Am. J. Sci. 268, 243–263.
Anderson, R.S., 1994. Evolution of the Santa Cruz Mountains, California, through tectonic growth and geomorphic decay. J. Geophys. Res. 99, 20,161–120,179.
Bierman, P.R., Nichols, K.K., 2004. Rock to sediment — slope to sea with 10Be — rates of landscape change. Ann. Rev. Earth Planet. Sci. 32, 215–255.
Bierman, P., Steig, E.J., 1996. Estimating rates of denudation using cosmogenic isotope abundances in sediment. Earth Surf. Processes Landf. 21, 125–139.
Binnie, S.A., Phillips, W.M., Summerfield, M.A., Fifield, L.K., 2007. Tectonic uplift, threshold hillslopes, and denudation rates in a developing mountain range. Geology 35, 743.
Blythe, A.E., Burbank, D.W., Farley, K.A., Fielding, E.J., 2000. Structural and topographic evolution of the central Transverse Ranges, California, from apatite fission-track, (U–Th)/He and digital elevation model analyses. Basin Res. 12, 97–114.
Brown, E.T., Stallard, R.F., Larsen, M.C., Raisbeck, G.M., Yiou, F., 1995. Denudation rates determined from the accumulation of in situ-produced ^{10}Be in the Luquillo Experimental Forest, Puerto Rico. Earth Planet. Sci. Lett. 129, 193–202.
Burbank, D.W., Leland, J., Fielding, E., Anderson, R.S., Brozovic, N., Reid, M.R., Duncan, C., 1996. Bedrock incision, rock uplift and threshold hillslopes in the northwestern Himalayas. Nature 379, 505–510.
Davis, W.M., 1892. The convex profile of badland divides. Science 20, 245.
DiBiase, R.A., Whipple, K.X., Heimsath, A.M., 2007. Channel morphology response to differential rock uplift rates in the San Gabriel Mountains, CA. EOS, American Geophysical Union Transactions, vol. 88. Abstract H41D-0760.
DiBiase, R.A., Heimsath, A.M., Whipple, K.X., 2008. Hillslope angle, channel steepness, and millenial erosion rates in the San Gabriel Mountains, CA. EOS, American Geophysical Union Transactions, vol. 89. Abstract H43F-1080.
Dietrich, W.E., Bellugi, D.G., Sklar, L.S., Stock, J.D., Heimsath, A.M., Roering, J.J., 2003. Geomorphic transport laws for predicting landscape form and dynamics. Prediction in Geomorphology Geophysical Monograph, vol. 135.
Dunai, T.J., 2000. Scaling factors for production rates of in situ produced cosmogenic nuclides: a critical reevaluation. Earth Planet. Sci. Lett. 176, 157–169.
Duvall, A., Kirby, E., Burbank, D., 2004. Tectonic and lithologic controls on bedrock channel profiles and processes in coastal California. J. Geophys. Res. 109. doi:10.1029/2003JF000086.
Finnegan, N.J., Roe, G., Montgomery, D.R., Hallet, B., 2005. Controls on the channel width of rivers: implications for modeling fluvial incision of bedrock. Geology 33, 229–232.
Flint, J.J., 1974. Stream gradient as a function of order, magnitude, and discharge. Water Resour. Res. 10, 969–973.
Gabet, E.J., 2003. Sediment transport by dry ravel. J. Geophys. Res. 108. doi:10.1029/2001JB001686.
Gilbert, G.K., 1877. Geology of the Henry Mountains, (Utah), Geographical and Geological Survey of the Rocky Mountains Region. U.S., Government Printing Office, Washington, D.C., US, p. 160.
Granger, D.E., Kirchner, J.W., Finkel, R.C., 1996. Spatially averaged long-term erosion rates measured from in situ-produced cosmogenic nuclides in alluvial sediment. J. Geol. 104, 249–257.
Hack, J.T., 1957. Studies of longitudinal stream profiles in Virginia and Maryland. U.S. Geological Survey Professional Paper, vol. 294-B, p. 97.
Hancock, G.S., Anderson, R.S., Whipple, K.X., 1998. Beyond power; bedrock river incision process and form. Geophys. Monogr. 107, 35–60.
Hanks, T.C., Bucknam, R.C., Lajoie, K.R., Wallace, R.E., 1984. Modification of wave-cut and faulting-controlled landforms. J. Geophys. Res. 89, 5771–5790.
Heimsath, A.M., 1999. The Soil Production Function. PhD thesis, University of California, Berkeley, 324 pp.
Heimsath, A.M., Dietrich, W.E., Nishiizumi, K., Finkel, R.C., 1997. The soil production function and landscape equilibrium. Nature 388, 358–361.
Heimsath, A.M., Furbish, D.J., Dietrich, W.E., 2005. The illusion of diffusion: field evidence for depth-dependent sediment transport. Geology 33, 949–952.
Hilley, G.E., Arrowsmith, J.R., 2008. Geomorphic response to uplift along the Dragon's Back pressure ridge, Carrizo Plain, California. Geology 36, 367–370.
Hovius, N., Stark, C.P., Allen, P.A., 1997. Sediment flux from a mountain belt derived by landslide mapping. Geology 25, 231–234.

Howard, A., 1994. A detachment-limited model of drainage basin evolution. Water Resour. Res. 30, 2261–2285.
Judson, S., Ritter, D.F., 1964. Rates of regional denudation in the United States. J. Geophys. Res. 69, 3395–3401.
Kirby, E., Whipple, K.X., 2001. Quantifying differential rock-uplift rates via stream profile analysis. Geology 29, 415–418.
Kirchner, J.W., Finkel, R.C., Riebe, C.S., Granger, D.E., Clayton, J.L., King, J.G., Megahan, W.F., 2001. Mountain erosion over 10 yr, 10 k.y., and 10 m.y. time scales. Geology 29, 591–594.
Kirkby, M.J., 1971. Hillslope process-response models based on the continuity equation. Inst. Br. Geogr. Spec. Pub. 3, 15–30.
Kobor, J.S., Roering, J.J., 2004. Systematic variation of bedrock channel gradients in the central Oregon Coast Range: implications for rock uplift and shallow landsliding. Geomorphology 62, 239–256.
Kohl, C.P., Nishiizumi, K., 1992. Chemical isolation of quartz for measurement of *in-situ*-produced cosmogenic nuclides. Geochim. Cosmochim. Acta 56, 3583–3587.
Lague, D., Davy, P., 2003. Constraints on the long-term colluvial erosion law by analyzing slope–area relationships at various tectonic uplift rates in the Siwaliks Hills (Nepal). J. Geophys. Res. 108. doi:10.1029/2002JB001893.
Lague, D., Hovius, N., Davy, P., 2005. Discharge, discharge variability, and the bedrock channel profile. J. Geophys. Res. 110. doi:10.1029/2004JF000259.
Langbein, W.B., Schumm, S.A., 1958. Yield of sediment in relation to mean annual precipitation. EOS., Am. Geophys. Union Trans. 39, 1076–1084.
Lavé, J., Burbank, D.W., 2004. Denudation processes and rates in the Transverse Ranges, southern California: erosional response of a transitional landscape to external and anthropogenic forcing. J. Geophys, Res. 109.
Lindvall, S.C., Rubin, C.M., 2008. Slip rate studies along the Sierra Madre-Cucamonga fault system using geomorphic and cosmogenic surface exposure age constraints: collaborative research with Central Washington University and William Lettis & Associates, Inc. US Geological Survey final report 03HQGR0084.
Matmon, A., Bierman, P.R., Larsen, J., Southworth, S., Pavich, M., Caffee, M., 2003. Temporally and spatially uniform rates of erosion in the southern Appalachian Great Smoky Mountains. Geology 31, 155–158.
Matti, J.C., Morton, D.M., 1993. Paleogeographic evolution of the San Andreas fault in southern California: a reconstruction based on a new cross-fault correlation. Geol. Soc. Amer.Mem. 178, 107–159.
Montgomery, D.R., Brandon, M.T., 2002. Topographic controls on erosion rates in tectonically active mountain ranges. Earth Planet. Sci. Lett. 201, 481–489.
Montgomery, D.R., Foufoula-Georgiou, E., 1993. Channel network source representation using digital elevation models. Water Resour. Res. 29, 3925–3934.
Morton, D.M., Miller, F.K., 2006. Geologic Map of the San Bernardino and Santa Ana 30′×60′ Quadrangles. US Geological Survey, California.
Niemi, N.A., Oskin, M., Burbank, D.W., Heimsath, A.J.M., Gabet, E.J., 2005. Effects of bedrock landslides on cosmogenically determined erosion rates. Earth Planet. Sci. Lett. 237, 480–498.
Ouimet, W.B., Whipple, K.X., Granger, D.E., 2009. Beyond threshold hillslopes: channel adjustment to base-level fall in tectonically active mountain ranges. Geology 37, 579–582.
Pelletier, J.D., Cline, M.L., 2007. Nonlinear slope-dependent sediment transport in cinder cone evolution. Geology 35, 1067–1070.
Penck, W., 1953. Morphological Analysis of Landforms: A Contribution to Physical Geology. Macmillan and Co., London.
Peterson, M.D., Wesnousky, S.G., 1994. Fault slip rates and earthquake histories for active faults in Southern California. Bull. Seismol. Soc. Am. 84, 1608–1649.
Roe, G.H., Montgomery, D.R., Hallet, B., 2002. Effects of orographic precipitation variations on the concavity of steady-state river profiles. Geology 30, 143–146.
Roering, J.J., Kirchner, J.W., Dietrich, W.E., 1999. Evidence for nonlinear, diffusive sediment transport on hillslopes and implications for landscape morphology. Water Resour. Res. 35, 853–870.
Roering, J.J., Kirchner, J.W., Sklar, L.S., Dietrich, W.E., 2001. Hillslope evolution by nonlinear creep and landsliding: an experimental study. Geology 29, 143–146.
Roering, J.J., Perron, J.T., Kirchner, J.W., 2007. Functional relationships between denudation and hillslope form and relief. Earth Planet. Sci. Lett. 264, 245–258.
Safran, E.B., Bierman, P.R., Aalto, R., Dunne, T., Whipple, K.X., Caffee, M., 2005. Erosion rates driven by channel network incision in the Bolivian Andes. Earth Surf. Processes Landf. 30, 1007–1024.
Schaller, M., von Blanckenburg, F., Hovius, N., Kubik, P.W., 2001. Large-scale erosion rates from in situ-produced cosmogenic nuclides in European river sediments. Earth Planet. Sci. Lett. 188, 441–458.
Schmidt, K.M., Montgomery, D.R., 1995. Limits to relief. Science 270, 617–620.
Schumm, S.A., 1963. The disparity between present rates of denudation and orogeny. U.S. Geol. Surv. Prof. Pap. 454-H.
Sklar, L., Dietrich, W.E., 1998. River longitudinal profiles and bedrock incision models: stream power and the influence of sediment supply. In: Tinkler, K.J., Wohl, E.E. (Eds.), Rivers Over Rock: Fluvial Processes in Bedrock Channels Geophysical Monograph Series 107. American Geophysical Union, Washington, D.C., pp. 237–260.
Sklar, L.S., Dietrich, W.E., 2004. A mechanistic model for river incision into bedrock by saltating bed load. Water Resour. Res. 40, W06301.
Sklar, L.S., Dietrich, W.E., 2006. The role of sediment in controlling steady-state bedrock channel slope: implications of the saltation–abrasion incision model. Geomorphology 82, 58–83.
Small, E.E., Anderson, R.S., Hancock, G.S., 1999. Estimates of the rate of regolith production using ^{10}Be and ^{26}Al from an alpine hillslope. Geomorphology 27, 131–150.
Snyder, N.P., Whipple, K.X., Tucker, G.E., Merritts, D.J., 2000. Landscape response to tectonic forcing: digital elevation model analysis of stream profiles in the Mendocino triple junction region, northern California. Geol. Soc. Am. Bull. 112, 1250–1263.
Snyder, N.P., Whipple, K.X., Tucker, G.E., Merritts, D.J., 2003. Importance of a stochastic distribution of floods and erosion thresholds in the bedrock river incision problem. J. Geophys. Res. 108, 2117.
Spotila, J.A., Farley, K.A., Sieh, K., 1998. Uplift and erosion of the San Bernardino Mountains associated with transpression along the San Andreas fault, California, as constrained by radiogenic helium thermochronometry. Tectonics 17, 360–378.
Spotila, J.A., House, M.A., Blythe, A.E., Niemi, N.A., Bank, G.C., 2002. Controls on the erosion and geomorphic evolution of the San Bernardino and San Gabriel Mountains, southern California. Geol. Soc. Am. Spec. Pap. 365, 205–230.
Stock, J., Dietrich, W.E., 2003. Valley incision by debris flows: evidence of a topographic signature. Water Resour. Res. 39.
Stock, G.M., Frankel, K.L., Ehlers, T.A., Schaller, M., Briggs, S.M., Finkel, R.C., 2008. Spatial and temporal variations in denudation of the Wasatch Mountains, Utah, USA. Lithosphere 1, 34–40.
Strahler, A.N., 1950. Equilibrium theory of erosional slopes approached by frequency distribution analysis. Am. J. Sci. 248 (673–696), 800–814.
Tucker, G.E., 2004. Drainage basin sensitivity to tectonic and climatic forcing: implications of a stochastic model for the role of entrainment and erosion thresholds. Earth Surf. Processes Landf. 29, 185–205.
Tucker, G.E., Bras, R.L., 1998. Hillslope processes, drainage density, and landscape morphology. Water Resour. Res. 34, 2751–2764.
Tucker, G.E., Bras, R.L., 2000. A stochastic approach to modeling the role of rainfall variability in drainage basin evolution. Water Resour. Res. 36, 1953–1964.
Tucker, G.E., Whipple, K.X., 2002. Topographic outcomes predicted by stream erosion models: sensitivity analysis and intermodel comparison. J. Geophys. Res. 107. doi:10.1029/2001JB000162.
Vanacker, V., von Blanckenburg, F., Hewawasam, T., Kubik, P.W., 2007. Constraining landscape development of the Sri Lankan escarpment with cosmogenic nuclides in river sediment. Earth Planet. Sci. Lett. 253, 402–414.
von Blanckenburg, F., 2005. The control mechanisms of erosion and weathering at basin scale from cosmogenic nuclides in river sediment. Earth Planet. Sci. Lett. 237, 462–479.
Whipple, K.X., 2004. Bedrock rivers and the geomorphology of active orogens. Ann. Rev. Earth Planet. Sci. 32, 151–185.
Whipple, K.X., Tucker, G.E., 1999. Dynamics of the stream-power river incision model: implications for height limits of mountain ranges, landscape response timescales, and research needs. J. Geophys. Res. 104, 17,661–617,674.
Whipple, K.X., Kirby, E., Brocklehurst, S.H., 1999. Geomorphic limits to climate-induced increases in topographic relief. Nature 401, 39–43.
Whipple, K.X., Hancock, G.S., Anderson, R.S., 2000. River incision into bedrock: mechanics and relative efficacy of plucking, abrasion, and cavitation. Geol. Soc. Am. Bull. 112, 490–503.
Wittmann, H., von Blanckenburg, F., Kruesmann, T., Norton, K.P., Kubik, P.W., 2007. Relation between rock uplift and denudation from cosmogenic nuclides in river sediment in the Central Alps of Switzerland. J. Geophys. Res. Earth Surf. 112.
Wobus, C., Whipple, K.X., Kirby, E., Snyder, N., Johnson, J., Spyropolou, K., Crosby, B., Sheehan, D., 2006. Tectonics from topography: procedures, promise, and pitfalls. Geol. Soc. Am. Spec. Pap. 398, 55–74.
Yanites, B.J., Tucker, G.E., Anderson, R.S., 2009. Numerical and analytical models of cosmogenic radionuclide dynamics in landslide-dominated drainage basins. J. Geophys. Res. 114. doi:10.1029/2008JF001088.
Yerkes, R.F., Campbell, R.H., 2005. Preliminary Geologic Map of the Los Angeles 30′×60′ Quadrangle. US Geological Survey, Southern California.